

Integrating mechanism-based T cell phenotypes into a model of tumor-immune cell interactions

Cite as: APL Bioeng. 8, 036111 (2024); doi: 10.1063/5.0205996

Submitted: 28 February 2024 · Accepted: 25 July 2024 ·

Published Online: 20 August 2024 · Corrected: 21 August 2024







View Online



Export Citation



CrossMark

Neel Tangella,¹  Colin G. Cess,²  Geena V. Ildefonso,²  and Stacey D. Finley^{1,2,3,a)} 

AFFILIATIONS

¹Department of Quantitative and Computational Biology, University of Southern California, Los Angeles, California 90089, USA

²Alfred E. Mann Department of Biomedical Engineering, University of Southern California, Los Angeles, California 90089, USA

³Mork Family Department of Chemical Engineering and Materials Science, University of Southern California, Los Angeles, California 90089, USA

Note: This paper is part of the special issue on Physical Sciences Approaches to Cancer Research.

^{a)}Author to whom correspondence should be addressed: sfinley@usc.edu

ABSTRACT

Interactions between cancer cells and immune cells in the tumor microenvironment influence tumor growth and can contribute to the response to cancer immunotherapies. It is difficult to gain mechanistic insights into the effects of cell–cell interactions in tumors using a purely experimental approach. However, computational modeling enables quantitative investigation of the tumor microenvironment, and agent-based modeling, in particular, provides relevant biological insights into the spatial and temporal evolution of tumors. Here, we develop a novel agent-based model (ABM) to predict the consequences of intercellular interactions. Furthermore, we leverage our prior work that predicts the transitions of CD8⁺ T cells from a naïve state to a terminally differentiated state using Boolean modeling. Given the details incorporated to predict T cell state, we apply the integrated Boolean–ABM framework to study how the properties of CD8⁺ T cells influence the composition and spatial organization of tumors and the efficacy of an immune checkpoint blockade. Overall, we present a mechanistic understanding of tumor evolution that can be leveraged to study targeted immunotherapeutic strategies.

© 2024 Author(s). All article content, except where otherwise noted, is licensed under a Creative Commons Attribution-NonCommercial 4.0 International (CC BY-NC) license (<https://creativecommons.org/licenses/by-nc/4.0/>). <https://doi.org/10.1063/5.0205996>

INTRODUCTION

The tumor microenvironment (TME) is a complex ecosystem comprised of many different cell types, including cancer cells and immune cells. It has long been shown that the immune system plays a pivotal role in tumor development.^{1–4} Although immune cells can detect malignant cells as “not-self” and then eliminate them, tumors are still able to grow and escape the immune system. In fact, in several cancer types, the TME has been shown to strongly contribute to the immunosuppressive state of the tumor.^{5,6} Furthermore, several studies point to the importance of the spatial location of stromal and immune cells in predicting prognosis and treatment response.^{7,8} Thus, by considering the composition and spatial structure of tumors, it may be possible to better understand the factors that drive tumor progression and the efficacy of anti-cancer treatments.⁹

Given its complexity, efforts to extensively explore the TME using *in vitro* and *in vivo* models alone are intractable. Fortunately, computational modeling is a useful approach to study the TME and understand how individual cell–cell interactions and changes at the molecular and

cellular levels influence tumor growth and response to treatment.¹⁰ For example, computational models have been used to better understand the interactions within the TME and predict how to improve immune-based cancer therapies.¹¹ A range of computational models have been developed to study various aspects of the TME and immunotherapy.^{12–15} Agent-based models (ABMs) have proven to be particularly useful,^{16–18} as they predict the spatial and temporal evolution of tumors and can simulate tumor behavior for a range of different conditions that are difficult and time-consuming to study using a purely experimental approach. Many ABMs exist and enable quantitative exploration of the TME. The level of detail included in the model depends on the specific question being addressed. For example, many ABMs use an entirely phenomenological framework to determine the cells’ behaviors.^{17,18} There are also examples of ABMs that embed networks inside of the agents to account for the role of intracellular features on cell behaviors.^{19–21} Here, we aim to study how transcriptional regulation of CD8⁺ T cells influences the cells’ state and properties such as killing ability and survival. Thus, we build on our prior work

using biophysical agent-based modeling to simulate tumor growth^{22–24} in a hybrid modeling framework by integrating our published Boolean model²⁵ of a gene regulatory network (GRN) with our existing rule-based ABM. The Boolean model simulates T cell evolution along a pseudo time trajectory providing valuable insight into transcriptional-level processes that influence emergent outcomes. This would not be possible with an ABM that only includes a rule-based approach to inform a cell's decision to proliferate, change phenotypic states, or induce cell killing. We predict the evolution of phenotypic T cell states, informed by the GRN encoded in the Boolean model. We consider three T cell states (naïve, pro-memory, and exhausted), which each have distinct properties. We apply the integrated model to study how CD8⁺ T cell state and properties influence tumor composition and spatial organization. Furthermore, we simulate immunotherapy via blockade of programmed cell death protein 1 (PD1), which is actively being pursued as a target to control tumor growth.^{26,27} By accounting for the GRN governing T cell behavior, which influences cell–cell interactions, we provide a mechanistic view of tumor evolution and a framework for predicting how tumor growth can be controlled via genetic alterations of T cells. Our model enables exploration of how targeted genetic alterations affect the TME.

RESULTS

We developed an ABM that captures the emergent outcomes associated with the interactions between cancer cells, cytotoxic CD8⁺ T cells, CD4⁺ T cells (T helper and T regulatory cells), and macrophages classed into three phenotypes (M0, M1, and M2). Cytotoxic CD8⁺ T cells can be in a pro-memory state or an exhausted state that has a higher probability of dying and is less cytotoxic compared to pro-memory CD8⁺ T cells. The cells and their interactions are depicted in Fig. 1. We include the cells' impact on differentiation and state changes [Fig. 1(a)]. Cancer cells and CD4⁺ T cells influence macrophage differentiation from the naïve state. Cancer cells and M2 macrophages influence differentiation of CD4⁺ T cells into T regulatory cells. The model also accounts for how other cells influence the killing and proliferation of CD8⁺ T cells [Figs. 1(b) and 1(c)].

Here, we use a novel model of tumor growth that integrates a GRN of CD8⁺ T cell states (predicted by a Boolean model) into an ABM that predicts cell-level behaviors and cell–cell interactions. This model leverages our prior work in simulating T cell state transitions.²⁵ Additionally, the ABM represents a significant expansion of our published modeling of cell–cell interactions within the tumor microenvironment.^{22–24} We apply the novel modeling framework to simulate tumor growth, with varying CD8⁺ T cell properties. We collect the two-dimensional position of cancer cells, T cells, and macrophages in an off-lattice setting, as well as cell-specific properties (radius, differentiation state, PDL-1 concentration in the case of cancer cells). We model TME evolution over a time period of 24 days starting from a small tumor mass located at the origin, and simulation data are logged once at the end of each simulated day. The model and its implementation are described in detail in the Methods section.

The rate of CD8⁺ T cell recruitment alters the number of cancer cells and relative proportions of immune cell subsets

We utilized this model and considered the baseline values for the probabilities of CD8⁺ T cell death and cancer cell killing and

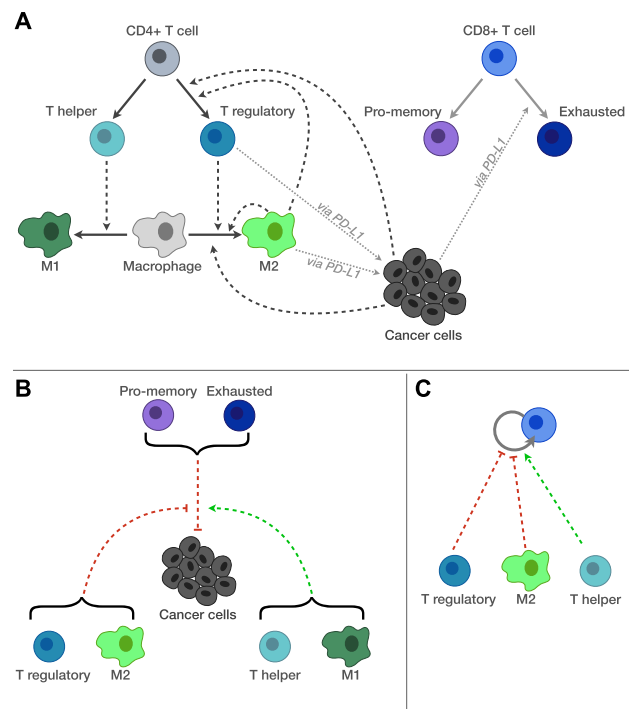


FIG. 1. Schematic of cell–cell interactions included in the ABM. (a) Cell state changes. (b) CD8⁺ T cell-mediated cancer cell killing. (c) CD8⁺ T cell proliferation. Solid lines indicate cell state transitions. Dashed lines indicate how cells influence one another: arrowhead, promotion; and bar, inhibition.

investigated the effects of the rate of CD8⁺ T cell recruitment. Overall, the model predicts tumor escape and the presence of pro-tumor immune cells for these CD8⁺ T cell properties. Panel (a) of Figs. 2 and 3 shows the number of cancer cells over time averaged over ten simulation replicates with a baseline and high CD8⁺ T cell recruitment, respectively, as well as the standard deviation. The model predicts that higher CD8⁺ T cell recruitment leads to fewer cancer cells (26 472 and 19 591 for base and high recruitment rates, respectively, at the end of the model simulation).

As shown in Figs. 2 and 3, the final numbers of macrophages are predicted to be slightly lower for high CD8⁺ T cell recruitment (8169 and 6664 macrophages for base and high recruitment rate, respectively). Furthermore, we can analyze the proportion of different types of a given cell type at the end of the simulation. Specifically, we define the macrophage compartment as consisting of macrophages in their naïve state (M0) as well as differentiated states (M1 and M2). The T cell compartment consists of CD8⁺ T cells in their naïve, pro-memory, and exhausted states as well as CD4⁺ T cells as T-helper or T-regulatory cells. We find the final relative proportion of macrophage types is only moderately impacted by the CD8⁺ T cell recruitment rate (Fig. 4). Specifically, pro-tumor macrophages comprise 79% of the macrophage population for baseline T cell recruitment, compared to 84% for fast T cell recruitment.

Furthermore, the number of exhausted CD8⁺ T cells increases by nearly fourfold (from 668 to 2641 for base and high T cell recruitment, respectively). This corresponds to differences in the relative

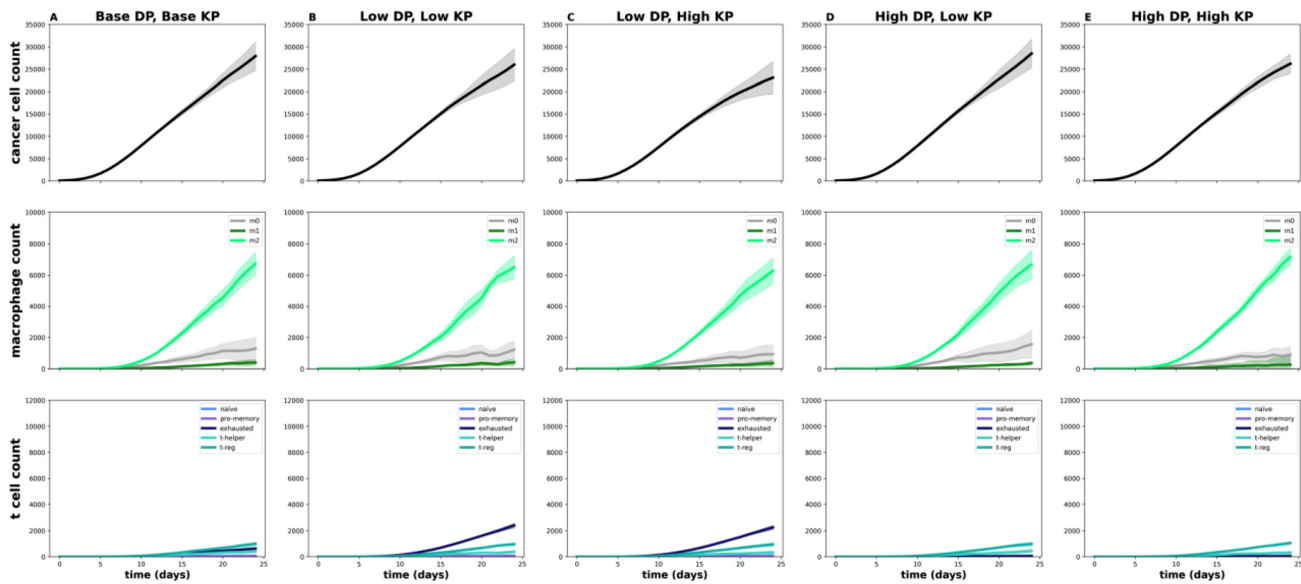


FIG. 2. Time courses of cell counts for various $CD8^+$ T cell properties, with base $CD8^+$ T cell recruitment rate. dp , probability of $CD8^+$ T cell death; kp , probability of $CD8^+$ T cell-mediated cancer cell killing. Note that the y-axes limits are set to enable direct comparison with Figs. 3, 8, and S2.

proportions of T cell subsets: 31% of $CD8^+$ T cells are in an exhausted state for a base recruitment rate, compared to 63% for a high recruitment rate (Fig. 5). In addition, $CD4^+$ T helper cells comprise 19% of the T cell compartment for baseline T cell recruitment, but only 7% for high T cell recruitment. These changes in the subsets of immune cells make sense, as faster $CD8^+$ T cell recruitment enables more T cells to enter the tumor; however, those T rapidly evolve toward the exhausted state. A larger proportion of exhausted $CD8^+$ T cells

corresponds to fewer $CD4^+$ helper cells, leading to fewer anti-tumor (M1) macrophages, due to T cell–macrophage interactions. We note that across both $CD8^+$ T cell recruitment rates, naive and pro-memory T cells represent less than 10% of the T cell compartment.

A useful feature of ABMs is their ability to predict the spatial organization of the cell populations being modeled. Thus, in addition to considering the time courses of the cell populations, we also examined the spatial layout at the end of the time course (Fig. 6) and over

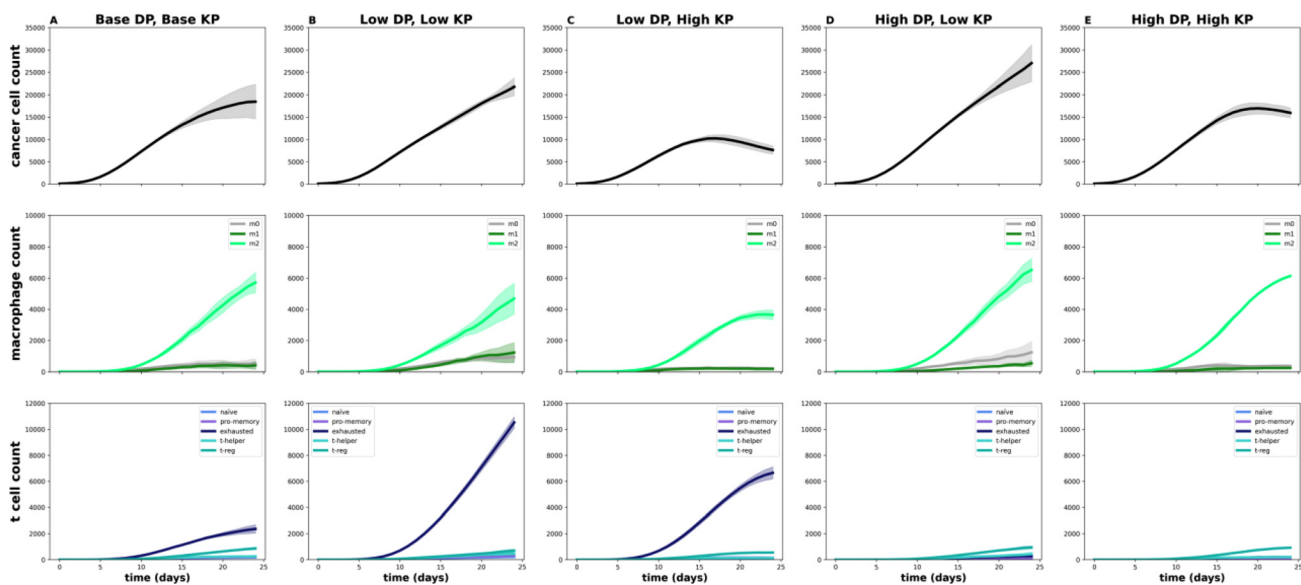


FIG. 3. Time courses of cell counts for various $CD8^+$ T cell properties, with high $CD8^+$ T cell recruitment rate. dp , probability of $CD8^+$ T cell death; kp , probability of $CD8^+$ T cell-mediated cancer cell killing. Note that the y-axes limits are set to enable direct comparison with Figs. 2, 8, and S2.

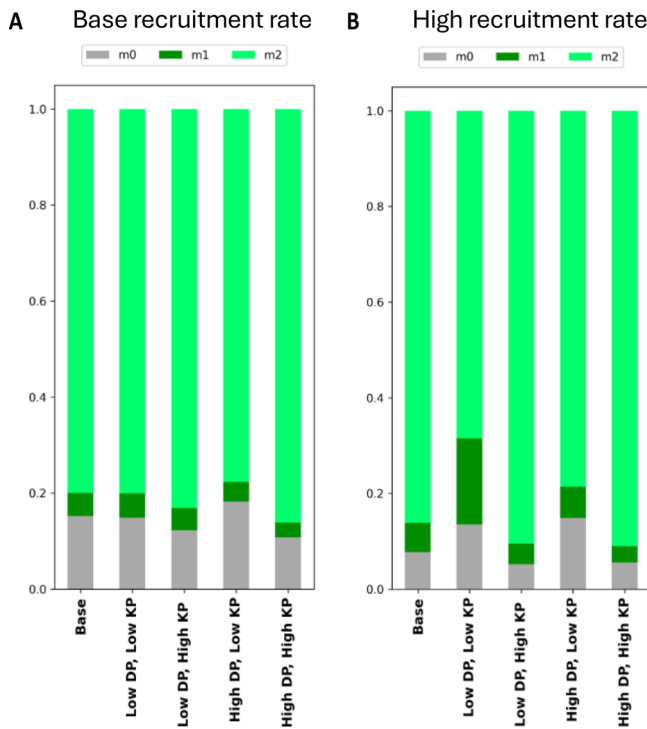


FIG. 4. Relative proportions of macrophages at the end of the model simulation for various CD8⁺ T cell properties. (a) Base CD8⁺ T cell recruitment rate. (b) High CD8⁺ T cell recruitment rate. *dp*, probability of CD8⁺ T cell death; *kp*, probability of CD8⁺ T cell-mediated cancer cell killing.

time (supplementary material, Movies 1 and 2). The predictions show that for both CD8⁺ T cell recruitment rates considered, there is minimal infiltration of CD8⁺ T cells, as they remain at the periphery of the tumor. This aligns with the concept of most tumors being classified as immunologically “cold,” defined as having low T cell infiltration.²⁸ The tumor periphery is also rich in macrophages. Additionally, there is moderate infiltration of macrophages into the tumor, and there is slightly less macrophage infiltration for the case of baseline CD8⁺ T cell recruitment rate. The model predicts that the average distance of

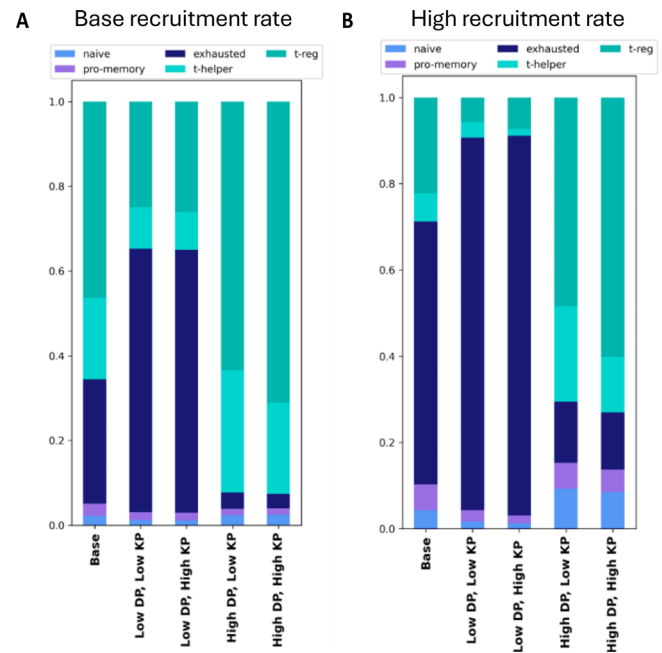


FIG. 5. Relative proportions of T cells at the end of the model simulation for various CD8⁺ T cell properties. (a) Base CD8⁺ T cell recruitment rate. (b) High CD8⁺ T cell recruitment rate. *dp*, probability of CD8⁺ T cell death; *kp*, probability of CD8⁺ T cell-mediated cancer cell killing.

macrophages from the tumor center is 1839 and 1544 μm for base and high recruitment rate, respectively (Table S1). Note that shorter distance from tumor center indicates more infiltration.

When CD8⁺ T cell recruitment is kept at a baseline, T cell death and cytotoxicity have differential effects on the number of cancer cells and the proportion of immune cells

The model predicts that the size of the cancer cell population is largely insensitive to the CD8⁺ T cell properties investigated. Here, we return to the analysis of the time courses shown in Fig. 2. The number

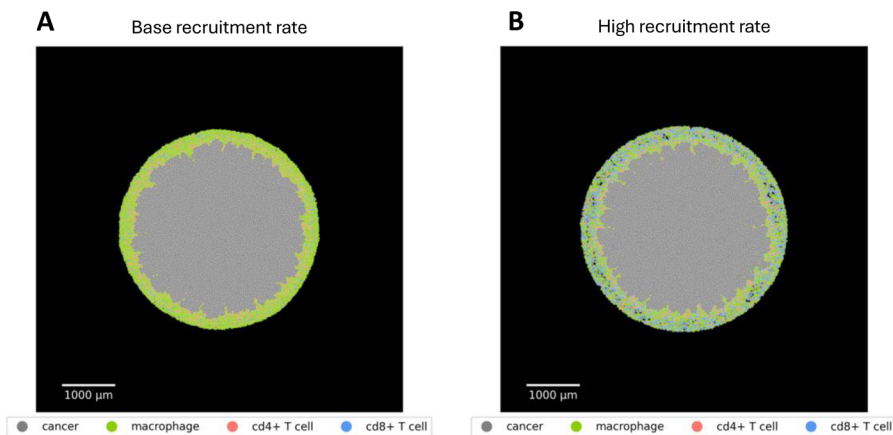


FIG. 6. Representative tumor spatial layouts for baseline model at the end of the simulation. (a) Base CD8⁺ T cell recruitment rate. (b) High CD8⁺ T cell recruitment rate.

of cancer cells increases exponentially for both low and high probability of $CD8^+$ T cell death, as well as the two probabilities of T cell-mediated cancer cell killing [Figs. 2(b)–2(e), top row]. Furthermore, the number of cancer cells present at the end of the simulation is approximately the same across all conditions. Similarly, the spatial organization of the tumor is consistent across $CD8^+$ T cell properties (supplementary material, Fig. S1).

In comparison, the number and relative proportions of macrophages depend on $CD8^+$ T cell properties. The model predicts increases in the number of pro-tumor macrophages over time for all four conditions [Figs. 2(b)–2(e), middle row]. When $CD8^+$ T cells have a low probability of cell-mediated cancer killing, M2 cells comprise 68%–80% of the macrophage compartment (Fig. 4). However, there are more M2 cells when the $CD8^+$ T cells have a high probability of T cell-mediated cancer cell killing, comprising 83%–85% of macrophages, for high or low probability of $CD8^+$ T cell death, respectively.

As anticipated, the probability of $CD8^+$ T cell death and the probability of inducing cancer cell killing influence the number of T cells [Figs. 2(b)–2(e), bottom row] and relative proportion of T cells in the tumor (Fig. 5). When $CD8^+$ T cells have a low probability of cell death, exhausted $CD8^+$ T cells, Tregs, and $CD4^+$ T helper cells make up approximately 62%, 21%–25%, and 9%–12% of the T cell population, respectively. In contrast, with high probability of $CD8^+$ T cell death, the proportion of exhausted $CD8^+$ T cell death is limited to 6% of all T cells. Having a smaller relative proportion of exhausted T cells corresponds to greater fractions of Tregs and T helper cells, ranging 61%–69% and 21%–28%, respectively, depending on the probability of T cell-mediated cancer cell killing. Again, these results can be traced to the cell–cell interactions included in the model. Having fewer pro-tumor macrophages (in the condition of high probability of T cell death) corresponds to more $CD4^+$ T helper cells, which promotes differentiation of naïve macrophages into the anti-tumor state (M1).

Overall, the model predicts that with a baseline recruitment of $CD8^+$ T cells, varying the properties of the $CD8^+$ T cells influences the number and proportions of immune cells, with only a minimal effect on the number of cancer cells. This is not an intuitive result, demonstrating the utility of a systems-level model of the tumor microenvironment.

High $CD8^+$ T cell recruitment permits tumor control and increases the relative size of the anti-tumor immune cell population

Across a range of values for the probability of $CD8^+$ T cell death and cancer cell killing probability, the final number of cancer cells is lower for fast $CD8^+$ T cell recruitment, compared to the baseline recruitment rate (Figs. 2 and 3, top row). One exception is the condition of a high probability of $CD8^+$ T cell death combined with a low probability of T cell-mediated killing [panel (d) in Figs. 2 and 3], as compared to the baseline rate of $CD8^+$ T cell recruitment.

The faster rate of $CD8^+$ T cell recruitment is predicted to influence the absolute number and relative proportions of macrophage and T cell subsets in the tumor. For all four conditions, the number of pro-tumor macrophages is lower when T cell recruitment is high (Figs. 2 and 3, middle row). Additionally, anti-tumor macrophages comprise a larger fraction of the macrophage population (4%–10% and 3%–8% for high and base recruitment rates, respectively), as shown in

Fig. 4. Furthermore, increasing $CD8^+$ T cell recruitment leads to a larger number (Figs. 2 and 3, middle row) and a greater proportion (Fig. 5) of exhausted $CD8^+$ T cells across all conditions. For example, exhausted $CD8^+$ T cells comprise 31% for the base T cell recruitment rate, compared to 63% for the case of high recruitment. These changes correspond to a smaller fraction of Tregs and greater percentage of pro-memory $CD8^+$ T cells. Altogether, the model predicts that higher $CD8^+$ T cell recruitment increases the proportion of anti-tumor immune cells (M1 and pro-memory $CD8^+$ T cells), concomitant with a decrease in the relative size of the anti-tumor T cell population (Tregs) and a nominal average decrease in anti-tumor macrophages (M2).

The spatial layout of the tumor further demonstrates the effect of increased $CD8^+$ T cell recruitment (Fig. 7). A comparison of the spatial organization of the tumor for base and high recruitment rates for a representative model output shows fewer cancer cells, with the exception of the case for the high probability of $CD8^+$ T cell death combined with low probability of T cell-mediated killing [Figs. 7(c) and 7(g)]. The tumors appear smaller, and we can visually appreciate the presence of substantially more exhausted $CD8^+$ T cells (colored blue). Additionally, there is greater infiltration of immune cells into the tumor when $CD8^+$ T cells are recruited at a faster rate and have a low probability of death [Figs. 7(e) and 7(g) and Table S1].

PD1 blockade increases the number of pro-memory $CD8^+$ T cells and enables better tumor control when T cell recruitment is high

Finally, we considered the effects of altering the intracellular GRN of $CD8^+$ T cells compared to the baseline model (termed wild-type, or “WT”). In particular, we simulated inhibition of PD1. Experimental studies demonstrate that blocking the PD1 pathway in naïve $CD8^+$ T cells during differentiation can alter the cell state transitions. As in our previous work, we implement the PD1 blockade by removing the ability of NFATC1 to activate PD1 in the Boolean model of the $CD8^+$ T cell GRN.

When $CD8^+$ T cells are recruited to the tumor at the base rate, the model predicts that inhibiting PD1 strongly decreases the absolute number of exhausted $CD8^+$ T cells, versus the WT case (compare the bottom rows of Figs. 2 and S1). Additionally, PD1 blockade significantly increases the proportion of pro-memory $CD8^+$ T cells [compare Fig. 5(a) to Fig. S1(b)]. Despite altering the composition of the T cell population, when $CD8^+$ T cell recruitment is at a baseline, a PD1 blockade does not affect the number of tumor cells or macrophages (compare the top two rows in Figs. 2 and S2). PD1 blockade also fails to alter the relative proportions of macrophages at the end of the model simulation [compare Fig. 4(a) to Fig. S1(a)].

In contrast, with higher $CD8^+$ T cell recruitment, the model predicts that PD1 blockade can lead to smaller tumors compared to WT with high T cell recruitment. In particular, for the base and low values of the probability of $CD8^+$ T cells considered, the numbers of tumor cells and pro-tumor macrophages are predicted to be lower than WT (compare the top two rows in Figs. 3 and 8). For example, with the baseline values for the probability of $CD8^+$ T cell death and T cell-mediated cancer cell killing, the number of cancer cells is 19 591 and 17 036 for the WT and PD1 blockade, respectively. However, the number of cancer cells also depends on $CD8^+$ T cell properties, even leading to more cancer cells with PD1 blockade. For example, when the

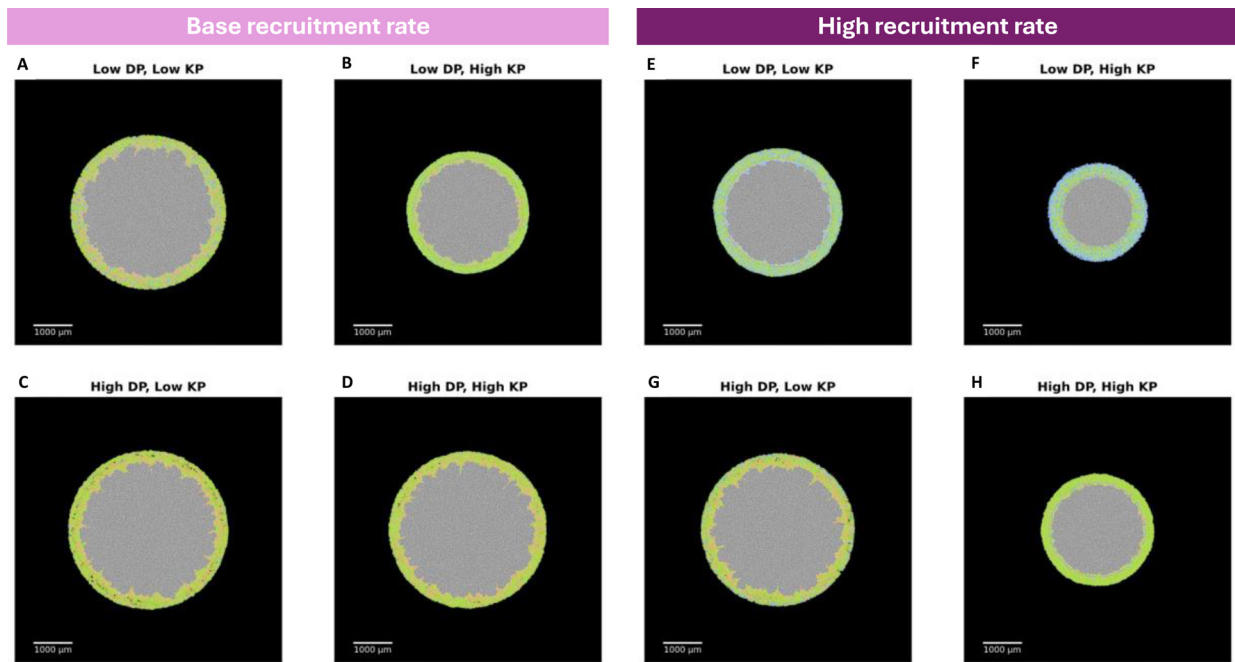


FIG. 7. Representative tumor spatial layouts for various $CD8^+$ T cell properties at the end of the simulation. (Left) Base $CD8^+$ T cell recruitment rate. (Right) High $CD8^+$ T cell recruitment rate. dp , probability of $CD8^+$ T cell death; kp , probability of $CD8^+$ T cell-mediated cancer cell killing. Gray, cancer cell; green, macrophage; red, $CD4^+$ T cell; and blue, $CD8^+$ T cell.

$CD8^+$ T cell death probability and killing probability are low, there are 18 245 and 20 867 cancer cells for WT and PD1 blockade, respectively. Interestingly, while the absolute numbers of M2 cells can decrease with PD1 blockade (compare the bottom row of Figs. 3 and 8), this does not

always correspond to a change in the final relative proportion of macrophages [compare Figs. 4(b) and 9(a)].

In contrast, PD1 blockade consistently increases the fraction of pro-memory $CD8^+$ T cells [compare Figs. 5(b) and 9(b)]. The

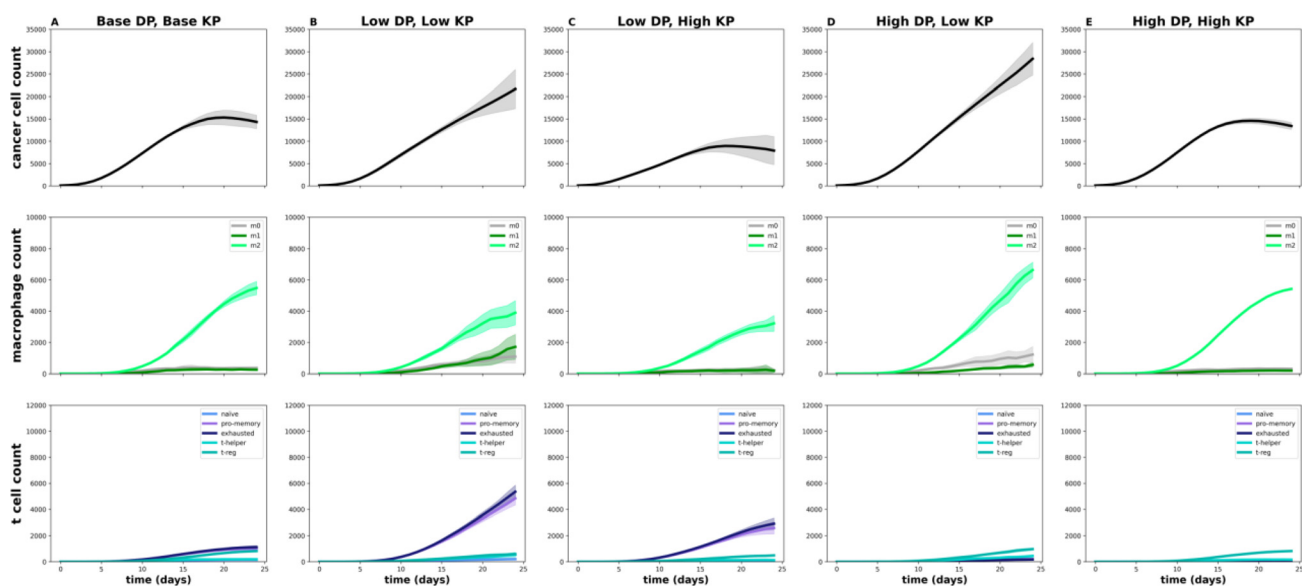


FIG. 8. Time courses of cell counts for various $CD8^+$ T cell properties, with high $CD8^+$ T cell recruitment rate and PD1 blockade implemented. dp , probability of $CD8^+$ T cell death; kp , probability of $CD8^+$ T cell-mediated cancer cell killing. Note that the y-axes limits are set to enable direct comparison with Figs. 2, 3, and S2.

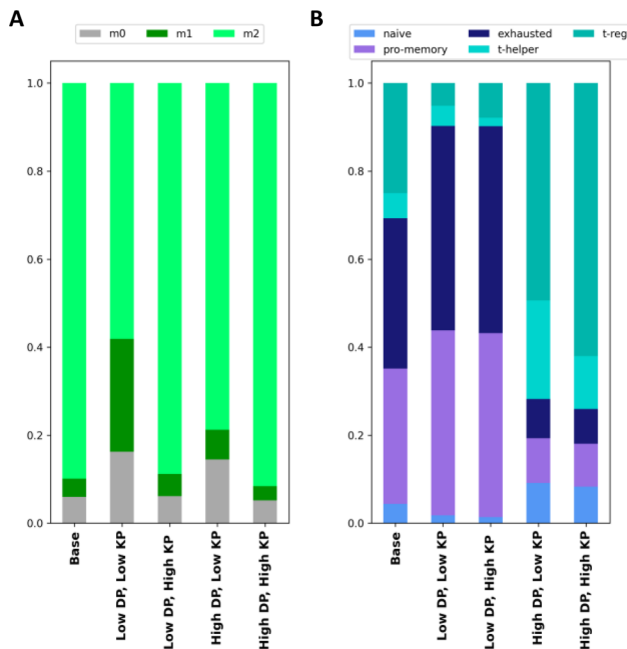


FIG. 9. Relative proportions of immune cells at the end of the model simulation for various CD8⁺ T cell properties, with high CD8⁺ T cell recruitment rate and PD1 blockade implemented. (a) Proportions of macrophages. (b) Proportions of T cells. *dp*, probability of CD8⁺ T cell death; *kp*, probability of CD8⁺ T cell-mediated cancer cell killing.

condition of having a low probability of CD8⁺ T cell death and high probability of T cell-mediated killing is an exemplary case. Here, the percentages of T cells in the pro-memory state at the end of the model simulation are 6% and 40%, respectively, for the WT and PD1 blockade cases. Visual inspection of the spatial layouts also demonstrates the effect of PD1 blockade (Fig. S4). We note that for a high probability of CD8⁺ T cell death, PD1 blockade is not able to reduce the number of cancer cells [the top row of Figs. 8(d) and 8(e)] despite there being more pro-memory CD8⁺ T cells. In summary, a combination of high CD8⁺ T cell recruitment and low CD8⁺ T cell death is needed for PD1 blockade to effectively control the size of the cancer cell population.

DISCUSSION

We have presented an agent-based modeling framework that predicts the spatiotemporal behavior of the tumor-immune ecosystem comprised of cancer cells and distinct subsets of macrophages and T cells. The model highlights that CD8⁺ T cell recruitment, their death, and cancer cell-mediated killing can influence tumor growth. Specifically, the combination of low T cell death probability and high T cell-mediated cancer killing most strongly controls tumor size with high T cell recruitment. In addition to predicting how the number of cancer cells evolves with time, our results consider the absolute number and relative proportions of macrophage and T cell subsets, representing the immune component of the tumor. Experimental and clinical studies demonstrate the efficacy of targeting the immune checkpoint inhibitor, PD1, to inhibit tumor growth.²⁷ Therefore, we applied the model to predict the effects of altering gene regulation

within CD8⁺ T cells to inhibit activation of the PD1 gene. This strategy is predicted to enhance the composition of the immune compartment, in agreement with published experimental studies. Given the mechanistic basis of our model, we can explain the efficacy of PD1 blockade, finding that it drastically shifts CD8⁺ T cells from an exhausted state to a pro-memory state. Importantly, the model shows that the efficacy of this PD1 blockade in controlling the number of cancer cells depends on CD8⁺ T cell properties. This result also aligns with experimental studies, where engineering CD8⁺ T cell characteristics is used to enhance the effects of immune checkpoint blockade.²⁹

A defining aspect of our work is the use of a Boolean model to inform the state transitions of CD8⁺ T cells. Specifically, we incorporate a Boolean representation of the GRN that mediates progression of CD8⁺ T cells from a naïve state to a terminally differentiated exhausted or pro-memory state.²⁵ The T cell's state influences its phenotype (probability of cell death) and cell-cell interactions (probability of promoting cancer cell killing). Thus, integration of the Boolean model allows the behaviors of CD8⁺ T cells in the ABM to be influenced by the intracellular gene regulation rather than taking a purely rule-based approach. The model also includes the effects of other cells on CD8⁺ T cell-mediated killing and death probability. We find that cell-cell interactions contribute to the final tumor composition (proportions of cancer and immune cells). With this modeling framework, we can simulate the effects of targeting interactions between cells. Furthermore, this integrated approach enables the investigation of targeted genetic strategies to alter a T cell's state. We have previously incorporated an intracellular network within an ABM to study the population-level effects of therapies that target macrophage intracellular signaling.²² Similarly, some ABMs consider intracellular models to inform the agent's behaviors.^{19,30,31} However, most ABMs use phenomenological rules to determine cell state changes and phenotypes. Thus, having a mechanistic basis for the CD8⁺ T cell behavior helps advance the field of agent-based modeling.

We acknowledge some areas for future improvements of this work. First, our model includes three classes of macrophages and five types of T cells. This is a vast simplification of the tumor-immune ecosystem. Thus, we can expand the model to include other immune subsets. For example, recent work reveals that interactions between T cells and dendritic cells influence T cell state changes and tumor growth.^{32,33} Related to this, we include differentiation of macrophages into just two broad classes (M1 and M2, anti- and pro-tumor, respectively); however, future work can consider a range of macrophage states and behaviors. Aligning the time steps simulated by the Boolean model is a second limitation of our work. We model that CD8⁺ T cells become exhausted within hours of stimulation by a cancer cell based on the findings of Rudloff and coworkers.³⁴ An issue with Boolean modeling is the use of pseudo-time, where the discrete time steps do not directly match real time. If the time required to reach an attractor state is known, one must assume what the interval between Boolean pseudo-time step corresponds to. For simplicity, we assume linear pseudo-time steps and that the Boolean model time steps correspond to a time interval of one hour. While the current work focuses on phenotypic features of CD8⁺ T cells, the effects of the time intervals within the Boolean model and aligning the timing between Boolean and ABM can be explored in future work. We can leverage the work of others in aligning timescales.^{30,35} Third, we note that altering the GRN that mediates CD8⁺ T cell state transitions may not happen with

100% efficiency in a heterogeneous population of cells. We can account for this by sampling from 10^4 simulated trajectories that are a mixture of WT and PD1 blockade. For example, assuming an alteration to the GRN within a population of cells is 80% effective, we would sample from a set of trajectories comprised of 2×10^3 WT and 8×10^3 PD1 blockade Boolean simulations. Finally, this work focuses on development of the integrated Boolean-ABM framework and explores how CD8⁺ T cell properties affect tumor growth. We have not performed a full analysis of the effect of varying all model parameters, a rigorous statistical analysis of model outputs, or a rigorous calibration of the model to tumor images from experimental models such as organoids or *in vivo* mouse tumors. Future work will leverage our recently developed machine learning-based approach to calibrate ABMs to such imaging data.²⁴

CONCLUSIONS

Taking an ecological view of a biological system by considering its spatial organization provides a framework for understanding the evolution of the system and the factors that control system behavior.³⁶ Similarly, in the context of cancer, by considering the composition and spatial structure of tumors, it may be possible to better understand the factors that drive tumor progression and response to treatment.⁹ We have demonstrated that biophysical agent-based modeling can produce biological insights into the tumor-immune ecosystem. Furthermore, accounting for the evolution of T cell states as determined by an intracellular model of CD8⁺ T cell gene activation simulates experimentally observed behaviors. Overall, our work provides a solid foundation for future studies to explore the role of cell-cell interactions in the TME and how they influence the response to treatment.

METHODS

Model description

Model overview

We develop an ABM to simulate the actions and interactions between cellular species in the TME. Specifically, we are able to capture the emergent outcomes associated with the interactions between cancer cells, cytotoxic CD8⁺ T cells (also referred to as CTLs), helper CD4⁺ T cells, and macrophages classed into three phenotypes (M0, M1, and M2). The cell-cell interactions are depicted in Fig. 1. This model provides a framework to develop sophisticated simulations of the TME and capture complex biophysical phenomena in simplified forms. We describe the model features below.

Cell forces

Cells are modeled using a center-based approach that considers each cell as a point and a radius; these two features are used to calculate physical forces between cells.^{23,37} This approach provides greater level of biological realism compared to grid-based approaches like the cellular-automata method. At the same time, the center-based approach is not as computationally expensive as frameworks that account for more detailed cell shapes such as the vertex model.³⁷ Intercellular forces are calculated via the following equation:

$$F_{i(t)} = \begin{cases} \mu_{ij}s_{ij}(t)\hat{x}_{ij}(t)\log\left(1 + \frac{\|x_{ij}(t)\| - s_{ij}(t)}{s_{ij}(t)}\right) & \text{for } \|x_{ij}(t)\| < s_{ij}(t), \\ \mu_{ij}\left(\|x_{ij}(t)\| - s_{ij}(t)\right)\hat{x}_{ij}(t)\exp\left(-k_c \frac{\|x_{ij}(t)\| - s_{ij}(t)}{s_{ij}(t)}\right) & \text{for } s_{ij}(t) \leq \|x_{ij}(t)\| \leq x_{max}, \\ 0 & \text{for } \|x_{ij}(t)\| > x_{max}. \end{cases}$$

In this equation, μ_{ij} is the spring constant, $x_{ij}(t)$ is the vector between cells i and j at time t , $\hat{x}_{ij}(t)$ is the unit vector, k_c is the decay of the attractive force, $s_{ij}(t)$ is the sum of the radii of cells i and j , and x_{max} is the maximum interaction distance. For all cells, we assume the same μ and k_c . This equation is solved numerically for each cell, as displayed in the following equation:

$$x_i(t + \Delta t) = x_i(t) + \frac{\Delta t}{\eta} \sum_{j \in \mathcal{N}_i(t)} F_{ij}(t).$$

Here, η is the drag coefficient, and \mathcal{N}_i is the set of cells within x_{max} of cell i . To preserve accuracy, this equation must be solved at a small time step (Δt), which we set as 0.005 h. The parameters x_{max} , η , μ , and k_c are taken from the literature and reported in Table S2.

When simulating the model, it is computationally expensive to determine $\mathcal{N}_i(t)$ for each cell, as the distances between each cell need to be calculated. To improve computational efficiency, we use a larger simulation time step of 1 h. This time step is both biologically realistic and computationally efficient. The reported time it takes for macrophages to respond to cytokines is on the order of hours.³⁸ However, to retain the accuracy of solving the force equation for every cell, we allow macrophage re-differentiation to occur every hour. At the beginning of each simulation step, we define a cell neighborhood for each cell. This is a list of cells with a $10x_{max}$ distance of cell i . We then determine $\mathcal{N}_i(t)$ only from cells in that neighborhood and proceed to solve the above-mentioned equation at the small time step. This hastens computational time while preserving the accuracy of the force calculations.

Proliferation and cell death

To simplify proliferation and cell death, these processes are modeled as probabilities of occurring at each time point. Cell proliferation is also influenced by the physical presence of other cells, assuming that cell proliferation is inhibited by excess physical forces.²³ We model the excess physical stress as being due to the “overlap” between the radii of adjacent cells. If the sum of the total overlap with other cells is above a threshold, a cell’s proliferation is inhibited until this overlap decreases. When a cell proliferates, the daughter cell is placed the distance of the cell radius away from the mother cell at a randomly selected angle. When a cell dies, it is removed from the simulation. Only cancer cells and CD8⁺ T cells can undergo proliferation.

Immune cell recruitment

Immune cells are recruited to the environment at a rate proportional to the number of cancer cells. They are recruited at a random angle around the tumor center, under the assumption that the area

surrounding the tumor is well vascularized. When recruited, these cells are placed a random distance away from the tumor edge, sampled from a uniform distribution (Table S2).

Immune cell migration

In the model, immune cells migrate toward tumor cells, mimicking chemotaxis due to tumor-secreted chemokines.^{39–41} Cells migrate with a specified amount of bias, which is modeled as the probability at each migration step of moving in the direction of the tumor center versus a random direction. This represents the impact of the extracellular matrix surrounding the tumor.^{42–46} However, there are many barriers to immune cell infiltration into the tumor, leading to three general tumor-immune states: ignored (immune cells cannot detect the tumor), inflamed (immune cells can infiltrate the tumor), and excluded (immune cells are restricted to the outside of the tumor).⁴⁷ Some of these are due to interactions between immune cells, while others are due to physical barriers of the tumor. To capture this phenomenon in a simplistic manner with as few additional parameters as possible, we assume that both migration speed and bias decrease upon entry into the tumor. By adjusting these decreases, this model can capture different phenotypic tumor behaviors. Migration for all immune cell types is modeled in the same way; however, each cell type has its own bias and speed parameters. CD4⁺ and CD8⁺ T cells have a comparable migration speed and bias, whereas macrophages have a reduced speed and increased bias compared to the T cells (Table S2).

Diffusion

Within the TME, cells can communicate via diffusible factors, such as cytokines.⁴¹ These are often modeled using PDEs, with cells acting as point sources/sinks.^{12,15,48} PDEs, however, require a great amount of computational time to solve, especially as environment size and the number of factors increases. Additionally, cells secrete several different cytokines, many with overlapping effects. This complexity makes it difficult to model the explicit biological effects of all the cytokines. Often, the effects of these factors are modeled either as a probability or a threshold value, instead of explicit modeling of downstream intracellular signaling. Because of this, researchers lump different cytokines into generic factors,⁴⁸ or replace diffusible factors with a distance threshold, where an effect occurs if one cell is within a specified distance from another cell.⁴⁹

Here, we implemented and extended the latter approach to better account for the gradient nature of diffusion and the impact of multiple secreting cells. We refer to this as the “cell influence,” where the closer cell i is to cytokine-secreting cell j , the greater the effect of cell j on cell i . This is modeled by an exponential decay displayed in the following equations:

$$D_{ij}(t) = \exp\left(-\lambda \|x_{ij}(t)\|\right),$$

$$\lambda = -\log_2(P_{th}) \frac{0.693}{x_{th}}.$$

The use of an exponential decay is a reasonable approximation of the effects of diffusible factors, as the response to a cytokine-secreting cell has been experimentally found to resemble an exponential decay.^{50,51} In these equations, $\|x_{ij}(t)\|$ is the distance between cell centers, x_{th} is the soft threshold for the maximum influence distance that can be

thought of as the diffusion limit, and P_{th} is the probability of an effect occurring at distance x_{th} . By setting P_{th} and x_{th} , we can calculate λ . The total influence on cell i is calculated via

$$D_{i,T}(t) = 1 - \prod_{j \in T(t)} (1 - D_{ij}(t)).$$

In this equation, $D_{i,T}(t)$ is the total influence, from 0 to 1, on cell i from all cells of cell type T . Thus, each cell records a separate influence for each cell type in the simulation. These influences are used to determine downstream effects. These downstream effects are probabilities, which are then multiplied by the relevant influence. Thus, the cell influence acts as a scaling factor for the probabilities of effects occurring. If two cell types can lead to the same effect, their influences are combined as

$$D(t) = 1 - (1 - D_{T_1})(1 - D_{T_2}).$$

This approach eliminates numerically solving PDEs and means that the cloud of diffusible factors follows each cell as it moves through the simulation environment. We followed the assumption that diffusion is resolved on a much faster timescale (seconds) than cellular processes (hours for cell division, for example).

Cancer cells

In this model, cancer cells have three main actions: proliferation, death, and expression of the PD1 ligand (PD-L1). Proliferation and death occur as described above. Cancer cells gain PD-L1 at a probability proportional to the influence from CD4⁺ helper cells (via T cell-secreted IFN- γ , which promotes PD-L1 expression) and M2 macrophages,^{12,52} dictated by the influence equation mentioned earlier. After proliferation, the daughter cells inherit the PD-L1 expression of the mother.

Macrophages

Classical *in vitro* characterization of macrophages leads to their classification into what have been called M2 pro-tumor and M1 anti-tumor macrophages. While it is now known that macrophages exist on a continuum, whereby their functions vary, and they can exhibit a range of phenotypes and functions,^{53,54} we retain these broad M1 and M2 groupings for the purpose of exploring the effects of anti- and pro-tumor macrophages.

Macrophages have a certain size⁵⁵ and enter the simulation in a naïve (M0) state and differentiate into either M1 (mimicking the response to IFN- γ secretion by CD4⁺ helper and CD8⁺ T cells) or M2 (mimicking the response to IL-4 and IL-10 secreted by cancer cells and Treg cells).⁵⁶ Additionally, because macrophage state is plastic and influenced by environmental conditions, macrophages have a probability of re-differentiating at each time step (1 h).⁵⁷ Following other modeling efforts, macrophages have a probability, p_i , of remaining in their current state (naïve, M1, or M2) or differentiating into M1 or M2 (influenced by environmental conditions). Specifically, p_i is the probability of transitioning to state M_i from any other state. Furthermore, these probabilities are then scaled to sum to 1.¹⁵ This is captured by the following equations, which utilize the cell influence described earlier,

$$p_0 = \begin{cases} 1 & \text{if } M_0, \\ 0 & \text{if not } M_0, \end{cases}$$

$$p_1 = 1 - (1 - D_{CD8})(1 - D_{CD4}),$$

$$p_2 = 1 - (1 - D_{M_2})(1 - D_{cancer})(1 - D_{T_{reg}}).$$

These values are then divided by their sum (p_{total}) to get the probability of differentiating into each state. Next, a random number is selected from a uniform distribution ranging from 0 to 1. If the number falls between 0 and p_0/p_{total} , the cell becomes M_0 . If the random number is between p_0/p_{total} and $(p_0 + p_1)/p_{total}$, the cell becomes an M_1 macrophage (or remains as M_1 if it is already in that state). If the random number falls between $(p_0 + p_1)/p_{total}$ and $(p_0 + p_1 + p_2)/p_{total}$, the cell becomes an M_2 macrophage (or remains as M_2 if it is already in that state).

M_2 cells promote the differentiation of $CD4^+$ T cells into the regulatory state (via IL-10 and TGF- β) and promote M_0 differentiation into the M_2 state (via TGF- β).^{56,58,59} We model all of these effects via the cell influence function described earlier. M_2 cells also express PD-L1.

CD4⁺ T cells

While $CD4^+$ T cells can take on a variety of states, for simplicity, we only model two: helper cells and regulatory cells. In this model, $CD4^+$ cells enter the simulation in the helper state and can be converted into regulatory cells based on influence from M_2 macrophages and cancer cells.^{56,58–60} The probability of differentiation is proportional to the combined influence of M_2 macrophages and cancer cells, as shown in the following equations:

$$D_{diff} = 1 - (1 - D_{M_2})(1 - D_{cancer}),$$

$$p_{diff} = p_{diff_0} D_{diff}.$$

In the helper state, $CD4^+$ cells promote M_0 differentiation into the M_1 state (via IFN- γ).⁶¹ As regulatory cells, they express CTLA-4 (which has the same function as PD-L1)⁶² and promote M_0 differentiation into the M_2 state (via IL-10).⁶⁰

CD8⁺ T cells

$CD8^+$ T cells serve the main function of killing cancer cells. In the TME, we consider a $CD8^+$ T cell to be in a naïve (N), exhausted (E), or pro-memory (M) state. $CD8^+$ T cells can undergo cell death, kill a neighboring cancer cell, and migrate.⁶³ The probability of a $CD8^+$ T cell dying or killing a cancer cell is influenced by (1) the $CD8^+$ T cell state and (2) the cells in its neighborhood. Specifically, we set the model parameter for each of these cell behaviors relative to a baseline set of behaviors. $CD8^+$ T cells in the N state are assumed to show no deviance from the base probabilities. In comparison, cells in the M state are half as likely to die and twice as likely to trigger cancer cell death, relative to baseline. Finally, $CD8^+$ T cells in the E state maintain the base probability of death; however, their ability to promote cancer cell killing is reduced by an order of magnitude, relative to baseline. By varying cell death and cytotoxicity, we capture $CD8^+$ T cell state-specific behaviors. The way in which the $CD8^+$ T cell's intracellular GRN influences the probability of a $CD8^+$ T cell dying or killing a cancer cell is detailed in the section “Integrating $CD8^+$ T cell

state decision into ABM.” Here, we describe how other cells in the TME influence $CD8^+$ T cell behaviors.

The model accounts for the effects of neighboring cells on $CD8^+$ T cell proliferation and the ability to kill cancer cells. Firstly, M_2 macrophages, T helper, and Treg cells impact $CD8^+$ T cell proliferation. The implementation follows the same approach of using the distance between cells to scale the cell probability,

$$D_{pos} = D_{Th},$$

$$D_{neg} = 1 - (1 - D_{M_2})(1 - D_{T_{reg}}),$$

$$p_{CD8_{prol}} = p_{CD8_{prol_0}}(D_{pos} - D_{neg}).$$

Second, the model includes the effect of PD-L1 expression by cancer cells on $CD8^+$ T cell-mediated killing by having cancer cells expressing PD-L1 to promote $CD8^+$ T cells to go to the exhausted state. Specifically, a number is randomly selected from a uniform distribution ranging from 0 to 1. If that random number is less than the PD-L1 expression (normalized from 0 to 1) on the cancer cell in contact with the $CD8^+$ T cell, the T cell will become exhausted. By being in the exhausted state, the T cell has reduced killing ability and higher probability of dying.

The model also accounts for the impact of macrophages and other T cell populations on $CD8^+$ T cells' killing ability. We consider the positive influence of M_1 macrophages and T helper cells on killing ability, and the negative influence of M_2 macrophages and Treg cells on killing ability. Specifically, the probability of $CD8^+$ T cell-mediated killing (p_{kill}) is positively and negatively influenced by the other immune cells, as shown in the following equations:

$$D_{pos} = 1 - (1 - D_{M_1})(1 - D_{Th}),$$

$$D_{neg} = 1 - (1 - D_{M_2})(1 - D_{T_{reg}}),$$

$$p_{kill} = p_{kill_0} \left(k_{scaling}^{(D_{pos} - D_{neg})} \right).$$

Here, p_{kill_0} is the baseline killing probability that is determined by whether the $CD8^+$ T cell is in the naïve, exhausted, or pro-memory state based on the intracellular gene regulatory network; D_i is the distance between the $CD8^+$ T cell and cell i , and $k_{scaling}$ is a scaling factor.

Defining the simulation loop

The simulation loop proceeds as follows (Fig. 10):

1. Immune cells are recruited to the environment.
2. Cell neighborhoods are determined.
3. Influence from cell–cell interactions due to proximity (mimicking the effects of diffusible factors) is calculated, direct contact effects ($CD8^+$ T cell-mediated cancer cell killing) are accounted for, $CD8^+$ T cell states are updated based on intracellular Boolean model.
4. Forces between cells are solved.
5. Species proliferation and spontaneous cell death are modeled.

Predicting $CD8^+$ T cell states

$CD8^+$ T cell state decisions were determined directly from the output of our previously published Boolean model of the GRN that defines $CD8^+$ T cell states.²⁵ This model predicts the expression profile

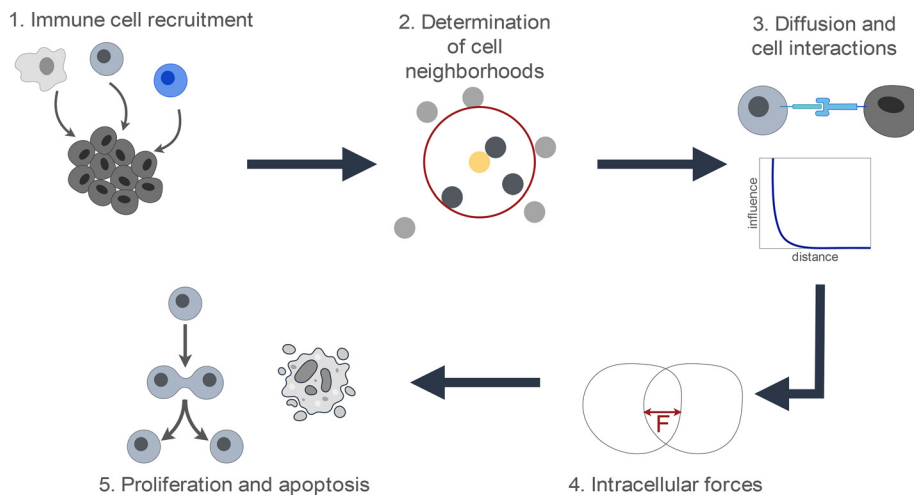


FIG. 10. Illustration of steps followed in the ABM simulation loop.

of $CD8^+$ T cell genes over pseudo-time. Although $CD8^+$ T cells occupy a continuum of phenotypes, we broadly class the cell's state into one of three main phenotypes: naïve (N), pro-memory (M), and exhausted (E), based on the output of the GRN predicted by the Boolean model. The model logs the on/off expression of 24 genes, where each gene is classified as promoting a proliferative pro-memory (PP) state or an effector exhausted (EE) state. The Boolean model predicts the state of each $CD8^+$ T cell at every time step based on the relative expression of PP and EE genes. Specifically, if more PP genes are *on* compared to EE, the phenotype is assumed to be M; the phenotype is assumed to be E if there are more EE genes *on* than PP. The first three pseudo-time steps are assumed to be in the N state; following stimulation of the T cell receptor, the predicted state in subsequent time steps is based on the expression of PP and EE genes.

For a single simulation, the output from a Boolean model simulation is given by an $n \times k$ matrix, where k represents the $CD8^+$ T cell state (N, P, or E) given by the rules described above, and n represents the number of time steps. Thus, moving down the rows of this matrix represents the “trajectory” that a cell takes in its evolution from a naïve state to the terminally differentiated state. Once a cell reaches its terminal state, it stays in that state for the remaining n time steps. Our prior work demonstrated that the Boolean model captures both linear differentiation of a T cell from M to E, and circular differentiation where the cell oscillates between M and E before reaching the final state.^{64,65}

Ten thousand simulations of the Boolean model were performed, representing a population of 10^4 distinct $CD8^+$ T cells. We first consider the baseline or wildtype (WT). We also considered the case where the $CD8^+$ T cell GRN encoded by the Boolean model reflects a PD1 blockade. Literature evidence shows that nuclear factor of activated T cells 1 (NFATC1) can promote antitumoral effector functions and memory $CD8^+$ T cell differentiation through regulation of PD1 expression upon T cell activation.^{66,67} Therefore, as described in our prior work,²⁵ we implemented indirect inhibition of PD1 via NFATC1. In the WT model, NFATC1 can activate PD1 (NFATC1 \rightarrow PD1), and here, we removed NFATC1 from the model, inhibiting PD1 activation. With this alteration of the GRN, 10^4 additional simulations of the Boolean model were performed to produce a population of 10^4 distinct $CD8^+$ T cells in which PD1 is inhibited.

Integrating $CD8^+$ T cell state decision into ABM

Updating ABM based on state predicted by Boolean model

The predicted $CD8^+$ T cell state given by the Boolean model transitions through pseudo-time. It is straightforward to initialize every $CD8^+$ T cell that is recruited to the tumor by sampling from the 10^4 trajectories produced by the Boolean model and assigning the selected trajectory to the $CD8^+$ T cell. However, we must assign a time interval for each pseudo-time step to align the transition of $CD8^+$ T cells states with the timescale of the ABM. Experimental evidence indicates that $CD8^+$ T cells become exhausted within hours following stimulation by a tumor cell.³⁴ We reflected this finding by updating the $CD8^+$ T cell state every hour. This would involve an assumption that each pseudo-time step of the Boolean model corresponds to one hour. Thus, the predicted $CD8^+$ T cell state given by the Boolean model at every time step is passed into the ABM. In the cases where the ABM time point is longer than the trajectory predicted by the Boolean (i.e., the $CD8^+$ T cell has reached its terminally differentiated state before the current ABM simulation timepoint), we assume the T cell remains in its final state (the last value in its trajectory predicted by the Boolean model) for the rest of the simulation until cell death. For PD1 inhibition, we instead initialize and update the states of $CD8^+$ T cells using the Boolean simulations corresponding to the altered GRN in which PD1 activation by NFATC1 is removed.

Assigning cell behavior based on state predicted by Boolean model

The “Model description” section details that $CD8^+$ T cells can die and kill cancer cells. The probability of each of these behaviors is determined by the state predicted by the Boolean model, relative to a base probability. $CD8^+$ T cells in the N state are assumed to show no deviance from the base probabilities. In comparison, cells in the M state are half as likely to die and twice as likely to trigger cancer cell death, relative to baseline. Finally, $CD8^+$ T cells in the E state maintain the base probability of death; however, their ability to promote cancer cell killing is reduced by an order of magnitude, relative to baseline. By

varying cell death and cytotoxicity, we capture CD8⁺ T cell state-specific behaviors.

Model implementation

This model is built in C++ using CMake for build processes. Scripts that develop the parameter grid as well as plotting scripts were implemented in Python. Two builds are presented, one developed for Apple Silicon and the other for a Unix-based computing cluster. The code is available at: <https://github.com/FinleyLabUSC/Boolean-TME-ABM>.

Model simulation

The parameter values used in the model are given in Table S2. We perform simulations to explore the effects of CD8⁺ T cell properties: recruitment rate (k_{recr}), probability of cell death (DP), and cancer cell killing probability (KP). We further investigate increased T cell recruitment (fivefold higher than the baseline value); varying the probability of cell death: fivefold increase and reduction in DP (high DP and low DP , respectively); and varying the probability of cancer cell killing: fivefold increase and reduction in KP (high KP and low KP , respectively). To account for variability in the predictions due to the probabilistic nature of the agent-based modeling, we performed ten replicates for each parameter combination considered.

SUPPLEMENTARY MATERIAL

See the [supplementary material](#) for supplementary figures and files. Movie 1 is representative of the time course of spatial layout over time for the baseline probabilities of CD8⁺ T cell death and cancer cell killing for base CD8⁺ T cell recruitment. Movie 2 is representative of the time course of spatial layout over time for the baseline probabilities of CD8⁺ T cell death and cancer cell killing for high CD8⁺ T cell recruitment. Table S1 provides the number and proportion of cell types, as well as mean infiltration distance for immune cells at the end of model simulations. Table S2 details the model parameters.

ACKNOWLEDGMENTS

We acknowledge the Finley research group for critical evaluation of this manuscript. This work was supported by the USC Center for Computational Modeling of Cancer.

AUTHOR DECLARATIONS

Conflict of Interest

The authors have no conflicts to disclose.

Ethics Approval

Ethics approval is not required.

Author Contributions

Neel Tangella: Formal analysis (lead); Investigation (lead); Methodology (lead); Software (equal); Writing – original draft (supporting); Writing – review & editing (supporting). **Colin G. Cess:** Methodology (supporting); Software (equal); Writing – review & editing (supporting). **Geena V. Ildefonso:** Methodology (supporting); Writing – review & editing (supporting). **Stacey D. Finley:**

Conceptualization (lead); Funding acquisition (lead); Resources (lead); Supervision (lead); Writing – original draft (equal); Writing – review & editing (lead).

DATA AVAILABILITY

The data that support the findings of this study are available within the article and openly available on GitHub at <https://github.com/FinleyLabUSC/Boolean-TME-ABM>, Ref. [68].

REFERENCES

- M. Binnewies, E. W. Roberts, K. Kersten, V. Chan, D. F. Fearon, M. Merad, L. M. Coussens, D. I. Gabrilovich, S. Ostrand-Rosenberg, C. C. Hedrick *et al.*, “Understanding the tumor immune microenvironment (TIME) for effective therapy,” *Nat. Med.* **24**, 541–550 (2018).
- D. Hanahan and L. M. Coussens, “Accessories to the crime: Functions of cells recruited to the tumor microenvironment,” *Cancer Cell* **21**, 309–322 (2012).
- D. S. Chen and I. Mellman, “Oncology meets immunology: The cancer-immunity cycle,” *Immunity* **39**, 1–10 (2013).
- D. C. Hinshaw and L. A. Shevde, “The tumor microenvironment innately modulates cancer progression,” *Cancer Res* **79**, 4557–4566 (2019).
- A. Kotsifaki, N. Alevizopoulos, V. Dimopoulou, and A. Armakolas, “Unveiling the immune microenvironment’s role in breast cancer: A glimpse into promising frontiers,” *Int. J. Mol. Sci.* **24**, 15332 (2023).
- V. G. Peddareddigari, D. Wang, and R. N. DuBois, “The tumor microenvironment in colorectal carcinogenesis,” *Cancer Microenviron.* **3**, 149–166 (2010).
- Y. Yuan, “Modelling the spatial heterogeneity and molecular correlates of lymphocytic infiltration in triple-negative breast cancer,” *J. R. Soc. Interface* **12**, 20141153 (2015).
- D. Georgopoulou, M. Callari, O. M. Rueda, A. Shea, A. Martin, A. Giovannetti, F. Qosaj, A. Dariush, S.-F. Chin, L. S. Carnevalli *et al.*, “Landscapes of cellular phenotypic diversity in breast cancer xenografts and their impact on drug response,” *Nat. Commun.* **12**, 1998 (2021).
- Y. Yuan, “Spatial heterogeneity in the tumor microenvironment,” *Cold Spring Harbor Perspect. Med.* **6**, a026583 (2016).
- G. L. Szeto and S. D. Finley, “Integrative approaches to cancer immunotherapy,” *Trends Cancer* **5**, 400–410 (2019).
- S. Z. Makaryan, C. G. Cess, and S. D. Finley, “Modeling immune cell behavior across scales in cancer,” *Wiley Interdiscip. Rev. Syst. Biol. Med.* **12**, e1484 (2020).
- C. Gong, O. Milberg, B. Wang, P. Vicini, R. Narwal, L. Roskos, and A. S. Popel, “A computational multiscale agent-based model for simulating spatio-temporal tumour immune response to PD1 and PDL1 inhibition,” *J. R. Soc. Interface* **14**, 20170320 (2017).
- P. S. Kim and P. P. Lee, “Modeling protective anti-tumor immunity via preventative cancer vaccines using a hybrid agent-based and delay differential equation approach,” *PLoS Comput. Biol.* **8**, e1002742 (2012).
- A. El-Kenawi, C. Gatenbee, M. Robertson-Tessi, R. Bravo, J. Dhillon, Y. Balagurunathan, A. Berglund, N. Visvakarma, A. Ibrahim-Hashim, J. Choi *et al.*, “Acidity promotes tumour progression by altering macrophage phenotype in prostate cancer,” *Br. J. Cancer* **121**, 556–566 (2019).
- G. Mahlbacher, L. T. Curtis, J. Lowengrub, and H. B. Frieboes, “Mathematical modeling of tumor-associated macrophage interactions with the cancer microenvironment,” *J. Immunother. Cancer* **6**, 10 (2018).
- K.-A. Norton, C. Gong, S. Jamalain, and A. S. Popel, “Multiscale agent-based and hybrid modeling of the tumor immune microenvironment,” *Processes* **7**, 37 (2019).
- J. Metzcar, Y. Wang, R. Heiland, and P. Macklin, “A review of cell-based computational modeling in cancer biology,” *JCO Clin. Cancer Inf.* **3**, 1–13 (2019).
- J. West, M. Robertson-Tessi, and A. R. A. Anderson, “Agent-based methods facilitate integrative science in cancer,” *Trends Cell Biol.* **33**, 300–311 (2023).
- R. W. Gregg, F. Shabnam, and J. E. Shoemaker, “Agent-based modeling reveals benefits of heterogeneous and stochastic cell populations during cGAS-mediated IFN β production,” *Bioinformatics* **37**, 1428–1434 (2021).

- ²⁰J. S. Yu and N. Bagheri, "Agent-based models predict emergent behavior of heterogeneous cell populations in dynamic microenvironments," *Front. Bioeng. Biotechnol.* **8**, 249 (2020).
- ²¹E. R. Reynolds, R. Himmelwright, C. Sanginiti, and J. O. Pfaffmann, "An agent-based model of the Notch signaling pathway elucidates three levels of complexity in the determination of developmental patterning," *BMC Syst. Biol.* **13**, 7 (2019).
- ²²C. G. Cess and S. D. Finley, "Multi-scale modeling of macrophage-T cell interactions within the tumor microenvironment," *PLoS Comput. Biol.* **16**, e1008519 (2020).
- ²³C. G. Cess and S. D. Finley, "Multiscale modeling of tumor adaption and invasion following anti-angiogenic therapy," *Comput. Syst. Oncol.* **2**, e1032 (2022).
- ²⁴C. G. Cess and S. D. Finley, "Calibrating agent-based models to tumor images using representation learning," *PLoS Comput. Biol.* **19**, e1011070 (2023).
- ²⁵G. V. Ildefonso and S. D. Finley, "A data-driven Boolean model explains memory subsets and evolution in CD8⁺ T cell exhaustion," *npj Syst. Biol. Appl.* **9**, 36 (2023).
- ²⁶M. A. Postow, M. K. Callahan, and J. D. Wolchok, "Immune checkpoint blockade in cancer therapy," *J. Clin. Oncol.* **33**, 1974–1982 (2015).
- ²⁷H. Li, P. A. van der Merwe, and S. Sivakumar, "Biomarkers of response to PD-1 pathway blockade," *Br. J. Cancer* **126**, 1663–1675 (2022).
- ²⁸S. Maleki Vareki, "High and low mutational burden tumors versus immunologically hot and cold tumors and response to immune checkpoint inhibitors," *J. Immunother. Cancer* **6**, 157 (2018).
- ²⁹J. Corria-Osorio, S. J. Carmona, E. Stefanidis, M. Andreatta, Y. Ortiz-Miranda, T. Muller, I. A. Rota, I. Crespo, B. Seijo, W. Castro *et al.*, "Orthogonal cytokine engineering enables novel synthetic effector states escaping canonical exhaustion in tumor-rejecting CD8⁺ T cells," *Nat. Immunol.* **24**, 869–883 (2023).
- ³⁰M. Ponce-de-Leon, A. Montagud, V. Noël, A. Meert, G. Pradas, E. Barillot, L. Calzone, and A. Valencia, "PhysiBoSS 2.0: A sustainable integration of stochastic Boolean and agent-based modelling frameworks," *npj Syst. Biol. Appl.* **9**(1), 54 (2023).
- ³¹S. M. Rikard, T. L. Athey, A. R. Nelson, S. L. M. Christiansen, J.-J. Lee, J. W. Holmes, S. M. Peirce, and J. J. Saucerman, "Multiscale coupling of an agent-based model of tissue fibrosis and a logic-based model of intracellular signaling," *Front. Physiol.* **10**, 1481 (2019).
- ³²D. Barras, E. Ghisoni, J. Chiffelle, A. Orcurto, J. Dagher, N. Fahr, F. Benedetti, I. Crespo, A. J. Grimm, M. Morotti *et al.*, "Response to tumor-infiltrating lymphocyte adoptive therapy is associated with preexisting CD8⁺ T-myeloid cell networks in melanoma," *Sci. Immunol.* **9**, eadg7995 (2024).
- ³³J. Duraiswamy, R. Turrini, A. Minasyan, D. Barras, I. Crespo, A. J. Grimm, J. Casado, R. Genolet, F. Benedetti, A. Wicky *et al.*, "Myeloid antigen-presenting cell niches sustain antitumor T cells and license PD-1 blockade via CD28 costimulation," *Cancer Cell* **39**, 1623–1642.E20 (2021).
- ³⁴M. W. Rudloff, P. Zumbo, N. R. Favret, J. J. Roetman, C. R. Detrés Román, M. M. Erwin, K. A. Murray, S. T. Jonnakuti, F. Dünder, D. Betel *et al.*, "Hallmarks of CD8⁺ T cell dysfunction are established within hours of tumor antigen encounter before cell division," *Nat. Immunol.* **24**, 1527–1539 (2023).
- ³⁵B. Aguilar, D. L. Gibbs, D. J. Reiss, M. McConnell, S. A. Danziger, A. Dervan, M. Trotter, D. Bassett, R. Hershberg, A. V. Ratushny *et al.*, "A generalizable data-driven multicellular model of pancreatic ductal adenocarcinoma," *GigaScience* **9**, g1aa075 (2020).
- ³⁶J. Friedman and J. Gore, "Ecological systems biology: The dynamics of interacting populations," *Curr. Opin. Syst. Biol.* **1**, 114–121 (2017).
- ³⁷J. M. Osborne, A. G. Fletcher, J. M. Pitt-Francis, P. K. Maini, and D. J. Gavaghan, "Comparing individual-based approaches to modelling the self-organization of multicellular tissues," *PLoS Comput. Biol.* **13**, e1005387 (2017).
- ³⁸T. D. Ricketts, N. Prieto-Dominguez, P. S. Gowda, and E. Ubil, "Mechanisms of macrophage plasticity in the tumor environment: Manipulating activation state to improve outcomes," *Front. Immunol.* **12**, 642285 (2021).
- ³⁹J. C. L. Alfonso, N. S. Schaadt, R. Schönmeier, N. Brieu, G. Forestier, C. Wemmert, F. Feuerhake, and H. Hatzikirou, "In-silico insights on the prognostic potential of immune cell infiltration patterns in the breast lobular epithelium," *Sci. Rep.* **6**, 33322 (2016).
- ⁴⁰J. C. Alfonso, G. D. Grass, E. Welsh, K. A. Ahmed, J. K. Teer, S. Pilon-Thomas, L. B. Harrison, J. L. Cleveland, J. J. Mulé, S. A. Eschrich *et al.*, "Tumor-immune ecosystem dynamics define an individual radiation immune score to predict pan-cancer radiocurability," *Neoplasia* **23**, 1110–1122 (2021).
- ⁴¹M. T. Chow and A. D. Luster, "Chemokines in cancer," *Cancer Immunol. Res.* **2**, 1125–1131 (2014).
- ⁴²P. Kameritsch and J. Renkawitz, "Principles of leukocyte migration strategies," *Trends Cell Biol.* **30**, 818–832 (2020).
- ⁴³F. Barros-Becker, P.-Y. Lam, R. Fisher, and A. Huttenlocher, "Live imaging reveals distinct modes of neutrophil and macrophage migration within interstitial tissues," *J. Cell Sci.* **130**, 3801–3808 (2017).
- ⁴⁴T. H. Harris, E. J. Banigan, D. A. Christian, C. Konradt, E. D. Tait Wojno, K. Norose, E. H. Wilson, B. John, W. Weninger, A. D. Luster *et al.*, "Generalized Lévy walks and the role of chemokines in migration of effector CD8⁺ T cells," *Nature* **486**, 545–548 (2012).
- ⁴⁵K. G. Anderson, I. M. Stromnes, and P. D. Greenberg, "Obstacles posed by the tumor microenvironment to T cell activity: A case for synergistic therapies," *Cancer Cell* **31**, 311–325 (2017).
- ⁴⁶H. Salmon and E. Donnadieu, "Within tumors, interactions between T cells and tumor cells are impeded by the extracellular matrix," *Oncoimmunology* **1**, 992–994 (2012).
- ⁴⁷D. Hammerl, J. W. M. Martens, M. Timmermans, M. Smid, A. M. Trapman-Jansen, R. Foekens, O. I. Isaeva, L. Voorwerk, H. E. Balcioğlu, R. Wijers *et al.*, "Spatial immunophenotypes predict response to anti-PD1 treatment and capture distinct paths of T cell evasion in triple negative breast cancer," *Nat. Commun.* **12**, 5668 (2021).
- ⁴⁸D. K. Wells, Y. Chuang, L. M. Knapp, D. Brockmann, W. L. Kath, and J. N. Leonard, "Spatial and functional heterogeneities shape collective behavior of tumor-immune networks," *PLoS Comput. Biol.* **11**, e1004181 (2015).
- ⁴⁹K. A. Norton, K. Jin, and A. S. Popel, "Modeling triple-negative breast cancer heterogeneity: Effects of stromal macrophages, fibroblasts and tumor vasculature," *J. Theor. Biol.* **452**, 56–68 (2018).
- ⁵⁰F. P. Assen and M. Sixt, "The dynamic cytokine niche," *Immunity* **46**, 519–520 (2017).
- ⁵¹A. Oyler-Yaniv, J. Oyler-Yaniv, B. M. Whitlock, Z. Liu, R. N. Germain, M. Huse, G. Altan-Bonnet, and O. Krichevsky, "A tunable diffusion-consumption mechanism of cytokine propagation enables plasticity in cell-to-cell communication in the immune system," *Immunity* **46**, 609–620 (2017).
- ⁵²S. Spranger, R. M. Spaepen, Y. Zha, J. Williams, Y. Meng, T. T. Ha, and T. F. Gajewski, "Up-regulation of PD-L1, IDO, and T_{regs} in the melanoma tumor microenvironment is driven by CD8(+) T cells," *Sci. Transl. Med.* **5**, 200ra116 (2013).
- ⁵³A. Mantovani, F. Marchesi, A. Malesci, L. Laghi, and P. Allavena, "Tumour-associated macrophages as treatment targets in oncology," *Nat. Rev. Clin. Oncol.* **14**, 399–416 (2017).
- ⁵⁴P. E. Gelbach and S. D. Finley, "Genome-scale modeling predicts metabolic differences between macrophage subtypes in colorectal cancer," *iScience* **26**, 107569 (2023).
- ⁵⁵F. Krombach, "Cell size of alveolar macrophages: An interspecies comparison," *Environ. Health Perspect.* **105**, 1261–1263 (1997).
- ⁵⁶A. Sica, P. Larghi, A. Mancino, L. Rubino, C. Porta, M. G. Totaro, M. Rimoldi, S. K. Biswas, P. Allavena, and A. Mantovani, "Macrophage polarization in tumour progression," *Semin. Cancer Biol.* **18**, 349–355 (2008).
- ⁵⁷S. K. Biswas and A. Mantovani, "Macrophage plasticity and interaction with lymphocyte subsets: Cancer as a paradigm," *Nat. Immunol.* **11**, 889–896 (2010).
- ⁵⁸A. J. Petty and Y. Yang, "Tumor-associated macrophages: Implications in cancer immunotherapy," *Immunotherapy* **9**, 289–302 (2016).
- ⁵⁹Y. Pan, Y. Yu, X. Wang, and T. Zhang, "Tumor-associated macrophages in tumor immunity," *Front. Immunol.* **11**, 583084 (2020).
- ⁶⁰M. Najafi, B. Farhood, and K. Mortezaee, "Contribution of regulatory T cells to cancer: A review," *J. Cell. Physiol.* **234**, 7983–7993 (2019).
- ⁶¹S. M. Liudahl and L. M. Coussens, "To help or to harm: Dynamic roles of CD4⁺ T helper cells in solid tumor microenvironments," in *Immunology*, edited by M. A. Hayat (Academic Press, 2018), Chap. 8, pp. 97–116.
- ⁶²J. F. M. Jacobs, S. Nierkens, C. G. Figdor, I. J. M. de Vries, and G. J. Adema, "Regulatory T cells in melanoma: The final hurdle towards effective immunotherapy?," *Lancet Oncol.* **13**, E32–E42 (2012).

- ⁶³S. N. Mueller, “Effector T-cell responses in non-lymphoid tissues: Insights from in vivo imaging,” *Immunol. Cell Biol.* **91**, 290–296 (2013).
- ⁶⁴A. N. Henning, R. Roychoudhuri, and N. P. Restifo, “Epigenetic control of CD8⁺ T cell differentiation,” *Nat. Rev. Immunol.* **18**, 340–356 (2018).
- ⁶⁵Y. Chen, R. Zander, A. Khatun, D. M. Schauder, and W. Cui, “Transcriptional and epigenetic regulation of effector and memory CD8 T cell differentiation,” *Front. Immunol.* **9**, 2826 (2018).
- ⁶⁶K. J. Oestreich, H. Yoon, R. Ahmed, and J. M. Boss, “NFATc1 regulates PD-1 expression upon T cell activation,” *J. Immunol.* **181**(7), 4832–4839 (2008).
- ⁶⁷L. Heim, J. Friedrich, M. Engelhardt, D. I. Trufa, C. I. Geppert, R. J. Rieker, H. Sirbu, and S. Finotto, “NFATc1 promotes antitumoral effector functions and memory CD8⁺ T-cell differentiation during non-small cell lung cancer development,” *Cancer Res* **78**, 3619–3633 (2018).
- ⁶⁸N. Tangella, C. G. Cess, and S. D. Finley (2004). “Boolean-TME-ABM,” GitHub. <https://github.com/FinleyLabUSC/Boolean-TME-ABM>